THREE-DIMENSIONAL FT*n* FINITE VOLUME SOLUTION OF SHORT-PULSE LASER PROPAGATION THROUGH HETEROGENEOUS MEDIUM

by

Kamel GUEDRI[a,b*], Mowffaq OREIJAH[a], Abdessattar BOUZID[c], Abdelaziz NASR[a], and Abdulmajeed S. Al-GHAMDI[a]

[a] Mechanical Engineering Department, College of Engineering and Islamic Architecture, Umm Al-Qura University, Makkah, Saudi Arabia
[b] UR: MEER, Faculty of Sciences of Gafsa, University of Gafsa, Gafsa, Tunisia
[c] Electrical Engineering Department, College of Engineering and Islamic Architecture, Umm Al-Qura University, Makkah, Saudi Arabia

Original scientific paper
https://doi.org/10.2298/TSCI180302186G

In this paper, 3-D heterogeneous medium, containing small inhomogeneous zones, subjected to a short-pulse laser has been examined by solving the transient radiative transfer equation. Both curved-line advection method and STEP schemes of the FTn finite volume method have been applied. The curved-line advection method predictions proved that a decrease of the false scattering and ray effects are obtained. In fact, there was a good agreement between the curved-line advection method and the Monte Carlo method. However, the STEP results are slightly mismatching the predictions of the aforementioned reference method. Then, the effects of the absorption coefficient, the size, the number and the position of inhomogeneous zone on the transmittance and reflectance signals have been analyzed. The predictions showed that the increase of the size of the inhomogeneity reduces the intensity of radiation. For both homogenous and heterogonous medium, the change of the detector position varies both the broadening of the signal pulse-width and the time with peak reflectance and/or transmittance. That is can be explained by the effects of the distance and the medium property between the laser-incident source and the detector position. Thus, these both parameters are the main factors for determining the peak position and the pulse broadening. Finally, the effects of the absorption coefficient in the inhomogeneity zone on the absolute values of logarithmic slope has been discussed. The results proved that the absolute values of logarithmic slope may be a perfect indicator for detecting any abnormal absorbing zones in the medium.

Key words*: short-pulse laser, heterogeneous medium, FTn finite volume, containing a small inhomogeneous zone, CLAM scheme*

Introduction

The study of short-pulse laser propagation through scattering and participating medium has received significant recent interest [1-4]. This technique is used in the processing of treatment of metallic materials [1], microstructures [2], laser surgery [3], and photodynamic therapy [4]. In addition, it can reduce the destruction adjacent healthy cells by its lower heat-affected zone [3, 4]. It is also applied to several high-precision medical treatments such as ophthalmology, neurosurgery, and corneal surgery [1-4].

* Corresponding author, e-mail: kamel.guedri@enim.rnu.tn

To study the effects of laser light on tissue phantoms, the solution of the transient radiative transfer equation (TRTE) is required. Recently, several numerical methods have been established to model the light propagation through participating tissues. The Monte Carlo [5-9], the integral equation (IE) formulation [10-12], and the discrete ordinates [13-15] methods have been developed to study the unsteady radiative heat transfer. The finite volume method (FVM) has been also developed and used [16-30]. Several researchers have demonstrated that he FVM has a respectable compromise between precision, flexibility, and moderate computational conditions [16-30]. It is also known by its compatibility with other methods applied in computational fluid dynamics. The FVM has been formulated and applied in several number of steady and transient radiative transfer cases [16-30]. However, the ray-effect and false scattering occurring in the FVM [20-30]. They are the two major discretization errors in the approximate FVM predictions for the TRTE.

High-order differencing spatial discretization schemes have been formulated to decrease the ray-effect. The MINMOD, CLAM, MUSCL, and SMART schemes have been proposed and tested for several benchmarks [23-30]. In another hand, the angular-multiblock technique has been proposed by Chai and Moder [28] and applied to decrease the false scattering. This procedure applies finer angular grids in optically thick zones. In addition, the non-uniform FT*n* FVM angular discretization has been formulated and examined for transient radiation transfer in participating scattering media [22-30]. The predictions proved that a decrease of the false scattering is obtained in 3-D cases and good agreements with the reference results are achieved. The results of the combination between the FT*n* FVM and the CLAM scheme proved that they produce more uniform distribution of the control-angles than the uniform FVM angular discretization. Thus, in this paper, the unsteady radiative transfer equation is solved using this combination of schemes to analyze the effects of a short-pulse laser subjected to a homogeneous and heterogeneous medium containing inhomogeneity zone, such as abnormal zones. The influences of the main optical parameters are examined.

Mathematical formulation

Transient radiative transfer equation

The biomedical tissue phantom scatters and absorbs the light. In this paper, a 3-D rectangular absorbing and scattering medium is considered. Both homogeneous and heterogeneous mediums are studied. Thus, when a short-pulse laser is subjected to this medium, the system is described by TRTE [31-33]:

$$\frac{1}{c_{med}}\frac{\partial I_d(\boldsymbol{r},\Omega,t)}{\partial t}+\frac{\partial I_d(\boldsymbol{s},\Omega,t)}{\partial s}=-\beta I_d(\boldsymbol{s},\Omega,t)+S_d(\boldsymbol{s},\Omega,t)+S_c(\boldsymbol{s},\Omega,t) \tag{1}$$

where $\beta = \sigma_a + \sigma_s$ is the extinction coefficient of the medium. The collimated and diffuse radiation terms are given:

$$S_c(\boldsymbol{r},\Omega,t)=\sigma_a I_b(\boldsymbol{s},t)+\frac{\sigma_s}{4\pi}\int_{4\pi} I_c(\boldsymbol{s},\Omega^{l'},t)\Phi(\Omega^{l'}\to\Omega^{l})\mathrm{d}\Omega^{l'} \tag{2}$$

$$S_d(\boldsymbol{r},\Omega,t)=\frac{\sigma_s}{4\pi}\int_{4\pi} I_d(\boldsymbol{s},\Omega^{l'},t)\Phi(\Omega^{l'}\to\Omega^{l})\mathrm{d}\Omega^{l'} \tag{3}$$

It is noted that the diffuse component of the intensity, I_d, that reaches the boundary of incidence marks in the reflectance, where the $I = I_d + I_c$ is the intensity in any general direction

Ω. The attenuation component of collimated radiation, I_c, and portion of the diffuse radiation, I_d, that arrives to the other boundary contribute to the transmittance.

In the aforementioned equations, I_b is the blackbody intensity, c_{med} is the speed of light in the medium, and t – the time, σ_a and σ_s define the absorption and the scattering coefficients of the medium, respectively, Φ – the scattering phase function and express the probability of a ray from one control angle, l', will be scattered into a certain other control angle, l. The intensity of the ultrafast laser, I_c, has a Gaussian expression in time and it is uniform in space [32]:

$$I_c\left(x=0,t\right)=I_0\exp\left[-4\ln(2)\left(\frac{t-3t_p}{t_p}\right)^2\right],\quad 0<t<6t_p \tag{4}$$

where I_0 is the maximum radiation intensity of the laser pulse, which happens at $t = 3t_p = 1.5/\beta c_{\text{med}}$. After $6t_p$, the medium is free from irradiation.

Discretization of the TRTE using the FTn FVM

In this paper, the FTn angular scheme of the finite volume method (FTn FVM) is applied. The FTn FVM used $n(n + 2)$ control angles and it subdivides the polar angle uniformly into an even number, n. However, the azimuthal angle is subdivided into the numbers of the arrangement of 4, 8, 12, ..., $2n$, $2n$, ..., 12, 8, 4 in each level of the polar angle [22-24, 29]. Thus, non-uniform control angles is obtained. In another hand, sevreal spatial discretization schemes may be applied to relate radiation intensities on the interfaces to the radiation intensity at the grid nodes. The CLAM scheme differs from the STEP scheme by the interpolation of intensities in a specified interface [22-25]. While the STEP scheme includes two grid nodes (one downstream node and one upstream node), the CLAM scheme used three grid nodes stencil: one downstream node and two upstream nodes. In the present formulation the previous schemes are investigated [22-24].

The Forward Euler scheme or the so-called the Explicit scheme, is a 1st order numerical procedure, in which the temporal dependent variable in the time instant ($t + \Delta t$) at a given point (as example for the TRTE: the radiation intensity at time instant $t + \Delta t$: $I^{t+\Delta t}$) can be calculated explicitly from the current time instant, t, solution values (as example for the TRTE: I^t), according to (for the TRTE example):

$$\frac{1}{c_{\text{med}}}\frac{\partial I}{\partial t}\approx\frac{I^{t+\Delta t}-I^t}{c_{\text{med}}\Delta t}=F\left(t,I^t\right) \tag{5}$$

where Δt is the time step and F is the temporal derivative of I at the instant t, divided by the propagation speed of light within the medium, c_{med}. This temporal scheme is easier to apply and computationally more efficient than the Backward Euler (Implicit) scheme, where the solution $I^{t+\Delta t}$ is determined by resolving a set of equations containing both the current and latter state. It is also mentioned that the explicit scheme needs a smaller time step Δt, by comparison the implicit scheme, in order to reach numerical stability. An in-house FORTRAN program was established. The discrete set of algebraic equations is resolved using tridiagonal matrix algorithm (TDMA) and an iterative procedure. The following convergence is applied:

$$\left\|\frac{|\,I_P^k-I_P^{k-1}\,|}{I_P}\right\|\le 10^{-5} \tag{6}$$

where k represents the number of iteration.

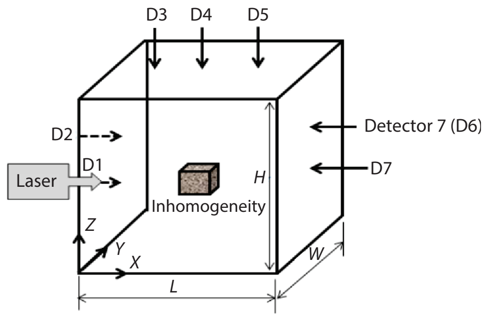

Figure 1. The 3-D medium containing inhomogeneity zone

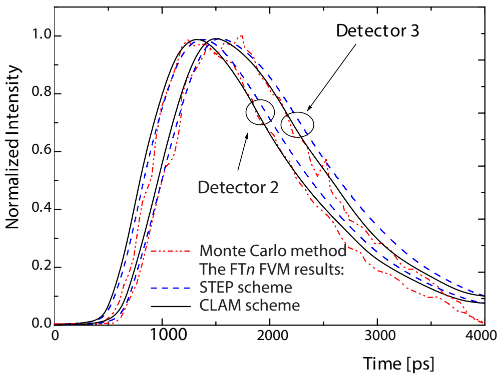

Figure 2. The temporal normalized intensity in 3-D medium model with a central inhomogeneity, 1.2 × 1.2 × 1.2 mm³ in size, σ_a = 0.10 mm⁻¹, the case of 3-D medium model with a central inhomogeneity, 1.2 × 1.2 × 1.2 mm³ in size, σ_a = 0.10 mm⁻¹

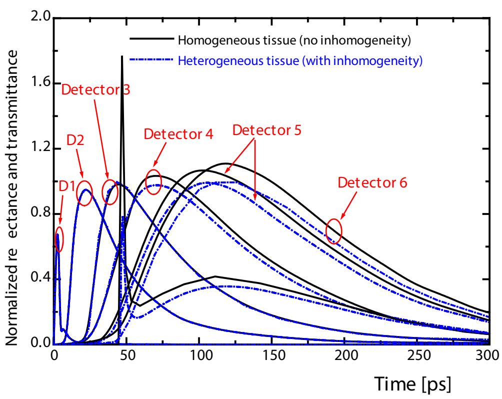

Figure 3. Temporal reflectance and transmittance signals for homogeneous and heterogonous mediums

Results and discussion

The developed in-house code, which represents a combination of the CLAM scheme and the FT*n* for spatial and angular discretizations of the TRTE, is examined for heterogeneous medium containing a small inhomogeneity zone. The effects of main optical parameters on transmittance and reflectance profiles are analysed.

Problem description

In this work, the present method is tested to study a short-pulse laser propagation through scattering cubic medium containing one or two small inhomogeneous zones.

Benchmark comparison

The cubic heterogeneous medium, with dimensions $L = W = H = 10$ mm and thermo-radiative properties $\sigma_a = 0.01$ mm^{-1} for the absorption coefficient and $\sigma'_s = 1.00$ mm^{-1} for the reduced-scattering coefficient [34], containing an inhomogeneity with dimensions of 1.2 × 1.2 × 1.2 mm³ fixed at its center, fig. 1. In the inhomogeneous zone, the reduced-scattering coefficient and the absorption coefficient are taken at $\sigma'_s = 1.00$ mm^{-1} and the absorption coefficient $\sigma_a = 0.10$ mm^{-1}.

The predictions of the temporal normalized intensity using the two proposed schemes of the FT*n* FVM are compared to the Monte Carlo solutions [35], in which the model resembles to the experimental predictions for ultrafast laser light interaction within medium, fig. 2. The results prove that the CLAM scheme are giving almost similar predictions as those of the Monte Carlo method. The STEP predictions are slight mismatching the solutions of the Monte Carlo method in both detector positions.

Effects of presence of the inhomogeneity zone

Figure 3 presents the effects of the presence of the inhomogeneity zone on the temporal adimensional reflectance and transmittance signals. It is mentioned that the profiles are normalized by their corresponding highest values in the inhomogeneous case at all detector positions. The homogeneous and the heterogeneous cases are obtained where the absorption coefficients of tumor are $\sigma_a = 0.01$ mm^{-1} and $\sigma_a = 0.50$ mm^{-1}, respectively.

Figure 3 displays the effects of the inhomogeneous zone on the temporal reflectance and transmittance. It is noted that both temporal signals are normalized by their corresponding highest values for the inhomogeneous case at all seven detector positions. In addition, in the homogeneous case the absorption coefficient of the inhomogeneity zone is the same as its value in the surrounding medium, *i. e.* $\sigma_a = 0.01$ mm^{-1}. However, in the case of an abnormality with an implanted fluorescent dye, $\sigma'_s = 0.50$ mm^{-1} is considered in the inhomogeneous zone. In this section only the CLAM predictions are discussed. For both homogenous and heterogonous mediums, fig. 3 shows that the change of the detector position varies both the broadening of the signal pulse-width and the time with peak reflectance and/or transmittance. That is can be explained by the effects of the distance and the medium property between the laser-incident source and the detector position. Thus, these parameters are the main factors for determining the peak position and the pulse broadening. The results prove that the time of peak position and the broadening of the pulse increase with the increase of the distance between the laser-incident point and the detector. From detector 1 to 3, the dissimilarity in the temporal profiles between the homogeneous media and the heterogeneous one is insignificant and it becomes clearer from detector 4 to 7.

Using the CLAM scheme, the comparison of absolute values of logarithmic slopes (AVLS) of the temporal reflectance and transmittance between normal homogeneous and inhomogeneous (with $\sigma_a = 0.5$ mm^{-1}) cases are displayed in fig. 4. The results of the AVLS converge to different constant values for homogeneous and inhomogeneous models, respectively. Such a difference in the AVLS between the two different medium cases is obvious at all 7 detector positions. The converged AVLS is only a function of the media property and it is approximately independent of the input laser pulse power.

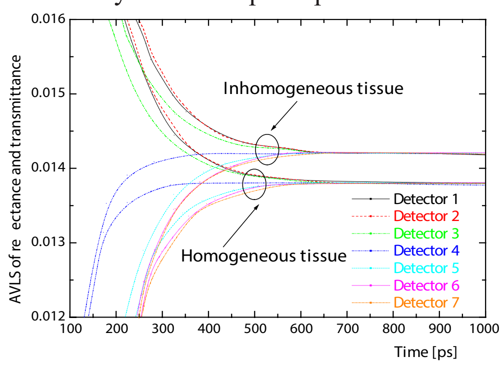

Figure 4. The AVLS of reflectance and transmittance for both homogeneous and heterogeneous models

Effects of the absorption coefficient of the inhomogeneity zone

All thermo-radiative and geometrical properties are those of the aforementioned section. However, here, the reduced-scattering coefficient in the inhomogeneous zone is taken at $\sigma'_s = 1.00$ mm^{-1} and four absorption coefficients, $\sigma_a = 0.01, 0.1, 0.2,$ and 0.50 mm^{-1}, are considered. For abnormal medium, the absorption coefficient of the inhomogeneity may change widely. Thus, fig. 5 shows the influence of this coefficient on the temporal trans-

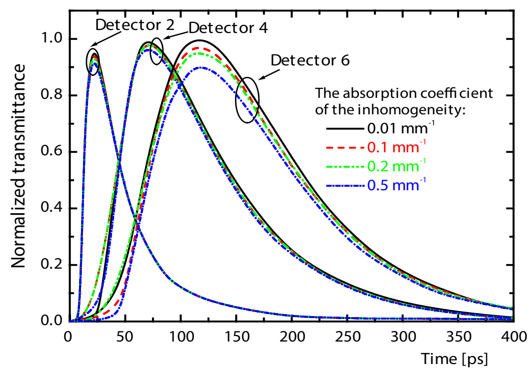

Figure 5. Effects the of absorption coefficient in the inhomogeneity zone on the temporal transmittance signals for the selected detectors 2, 4, and 6

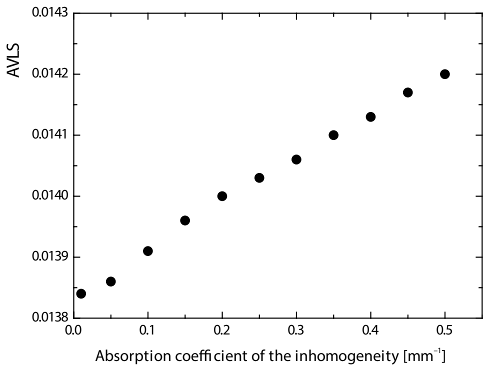

Figure 6. Relationship between AVLS and absorption coefficient of the inhomogeneity

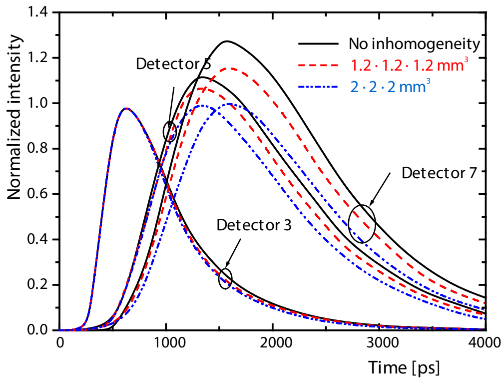

Figure 7. Effects of the size of the inhomogeneity zone on the temporal of normalized intensities

mittance using the CLAM scheme. It is shown that the amplitudes of the signals for detectors, 2, 4, and 6 are reduced by increasing σ_a. In addition, this increase widens the difference in the signals between the homogeneous and heterogeneous models. Even with a slight rise of absorption (*e. g.*, $\sigma_a = 0.05$ mm^{-1}), the difference is still observable.

The effects of the absorption coefficient of the inhomogeneity on the AVLS is manifested in fig. 6. The AVLS is almost linearly proportional to this coefficient as proved by the predictions for the selected detectors 2, 4, and 6. This AVLS can be a perfect sign to detect any inhomogeneity. Such a discovery presented here for inhomogeneous medium containing small inhomogeneity zones may be explored for early finding of malignant in biomedical tissue.

Effects of the size of the inhomogeneity zone

In this section, three test cases, no inhomogeneity, a 1.2 × 1.2 × 1.2 mm^3 inhomogeneity, and a 2 × 2 × 2 mm^3 inhomogeneity are considered to evaluate the performance of the FT*n* FVM. The absorption coefficient of the inhomogeneity is fixed at 0.5 mm^{-1}. Figure 7 presents the normalized intensities results for the selected detectors 3, 5, and 7.

The increase of the size of the inhomogeneity zone reduces the intensity of radiation, fig. 7. In fact, the large inhomogeneity (2 × 2 × 2 mm^3) situation produces the smallest value, thus its intensity of radiation is reserved as the reference for comparison, fig. 7. The predictions proved that the size variation of inhomogeneity does not affect significantly the predictions in detector position 1. This can be explained by the fact that the interval between the source and this detector is not directly affected by the presence of the inhomogeneous zone. A strong influence of the intensity of radiation in detector positions 2 and 3 is obtained because the inhomogeneity is introduced between the source and these detectors.

Effects of the number and position of the inhomogeneity zone

In this section two inhomogeneity zones are investigated: one high absorption zone (with $\sigma_a = 0.5$ mm^{-1}) and one low absorption zone (with $\sigma_a = 0.05$ mm^{-1}) are placed at the top-right and bottom-left corners of the base medium, fig. 8, respectively. Both inhomogeneity zones have the same size 2 × 2 × 2 mm^3. For detector positions 5, 7, and 8, the effects of tse zones on the temporal of normalized intensities profiles are showed in fig. 9. By comparison with the single and central inhomogeneity model, the predictions of the detector 7 for dual-inhomogeneity positions are not clearly different from those for homogeneous medium because the two inhomogeneity positions are very far away from this detector in this case. However, the results of detector 5 are more affected in the case of two inhomogeneities as compared to the previous single-inhomogeneity model predictions. In another hand, it is shown that the STEP solutions will predict improper results when the detector is close to the highly absorbing inhomogeneity region due to the large false scattering obtained when this scheme is applied. Thus, a mesh refinement is required. However, the CLAM scheme produces quantitative and qualitative predictions due to its high accuracy and its lower false scattering.

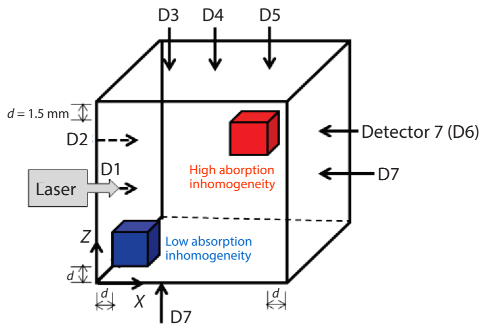

Figure 8. The 3-D medium containing dual-inhomogeneity zones

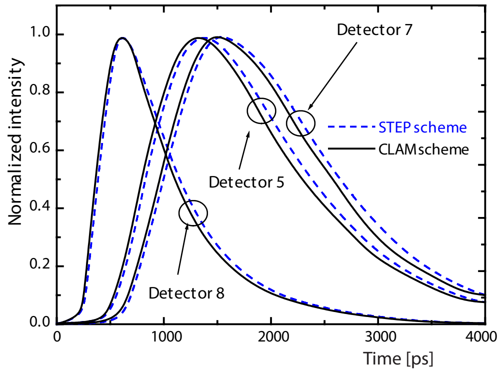

Figure 9. The temporal of normalized intensities for the case of dual-inhomogeneity zones

Conclusion

In this work, 3-D medium subjected to a short-pulse laser has been examined using the FTn FVM. Both the CLAM and STEP schemes have been applied to discretize the TRTE. Heterogeneous medium containing small inhomogeneous zones have been considered. The present predictions are confirmed by comparison with Monte Carlo reference solutions. The CLAM predictions proved that a decrease of the false scattering and ray effects have been obtained. Thus, good agreements with the reference results have been achieved. However, the STEP results are slightly mismatching the solutions of the reference method. The influence of the absorption coefficient, the size, the number and the position of the inhomogeneity zone on the reflectance and transmittance signals have been analyzed. The effect of the absorption coefficient in the inhomogeneity zone on the AVLS has been discussed. The results proved that this AVLS can be a good sign to detect any inhomogeneity zones. Such a discovery presented here for inhomogeneous medium containing small inhomogeneity zones may be explored for early finding abnormal zone in the medium. Further complete theoretical and numerical search will survey in the next phase of this work to response this important goal of this paper.

Acknowledgment

The paper contains the results and findings of a research project that is funded by King Abdulaziz City for Science and Technology (KACST) Grant No. SG-36-90. The researchers express their gratitude and appreciation KACST for providing this research grant.

Nomenclature

c_{med} – the speed light in the medium, [ms^{-1}]
I – intensity, [Wm^{-2}sr^{-1}]
I_b – black body intensity, [Wm^{-2}sr^{-1}]
I_d – diffuse radiation, [Wm^{-2}sr^{-1}]

I_c – collimated intensity, [Wm^{-2}sr^{-1}]
I_0 – the maximum radiation intensity, [Wm^{-2}sr^{-1}]
n – the refractive index of the medium, [–]
S_c – source term due to collimated radiation
S_d – source term due to diffuse radiation
$\boldsymbol{s}$ – geometric distance, [m]
t – time, [s]

Greek symbols

β – extinction coefficient, [m^{-1}]
σ_a – absorption coefficient, [m^{-1}]
σ_s – scattering coefficient, [m^{-1}]
Ω – unit vector in direction of intensity

Superscripts

l, l' – discrete angular directions

References

[1] Shibib, K. S., *et al*., Finite Element Analysis of Spot Laer of Steel Welding Temperature History, *Thermal Science*, *13* (2009), 4, pp. 143-150
[2] Sazgarnia, A., *et al*., Investigation of Thermal Distribution for Pulsed Laser Radiation in Cancer Treatment with Nanoparticle-Mediated Hyperthermia, *Journal of Ther. Biology*, *47* (2015), Jan., pp. 32-41
[3] Tahir, M. M., Threshold of Permanent Cornea Thermal Damage Due to Incidental Continuous Wave CO_2 Laser Irradiation, *Thermal Science*, *14* (2010), 2, pp. 459-467
[4] Havermann, M., Beylich, A. E., Performance and Limitations of the Laser-Induced Fluorescence Measurement Technique and the Established Experimental Methods or the Study of Supersonic Mixing, *International Journal of Heat and Technology*, *15* (1997), 2, pp. 3-10
[5] Guo, Z., Hunter, B., Modelling of Ultrafast Laser Transport and Applications, *Proceedings*, 8th International Symposium on Heat Transfer, Beijing, China, 2012
[6] Wang, L., *et al*., Monte Carlo Modelling of Light Transport in Multi-Layered Tissues, *Computer Methods and Programs in Biomedicine*, *47* (1995), 2, pp. 131-146
[7] Ratovoson, D., *et al*., Combined Model of Human Skin – Heat Transfer in the Vein and Tissue: Experimental and Numerical Study, *Quant. Infrared Thermography J*., *8* (2012), 2, pp. 165-186
[8] Guo, Z., *et al*., Multidimensional Monte Carlo Simulation of Short-Pulse Laser Transport in Scattering Media, *AIAA J. Thermophys Heat Transfer*, *144* (2000), 4, pp. 504-511
[9] Jang, C., *et al*., Radiative Heat Transfer Analysis in Pure Scattering Layers to Be Used in Vacuum Insulation Panels, *Applied Energy*, *112* (2013), Dec., pp. 703-709
[10] Tan, Z. M., Hsu, P. F., An Integral Formulation of Transient Radiative Transfer, *ASME Journal Heat Transfer*, *123* (2011), 3, pp. 466-475
[11] Wu, S. H., Wu, C. Y., Time-Resolved Spatial Distribution of Scattered Radiative Energy in a 2-D Cylindrical Medium with a Large Mean Free Path for Scattering, *International Journal of Heat and Mass Transfer*, *44* (2001), 14, pp. 2611-2619
[12] Wu, S. H., Wu, C. Y., Integral Equation Solutions for Transient Radiative Transfer in Non-Homogeneous Anisotropically Scattering Media, *ASME J. Heat Transfer*, *122* (2000), 4, pp. 818-822
[13] Chen, T. H., *et al*., Combined Natural-Convection and Radiation with Temperature-Dependent Properties, *Thermal Science*, *22* (2018), 2, pp. 921-930
[14] Hunter, B., Guo, Z., Numerical Smearing, Ray Effect, and Angular False Scattering in Radiation Transfer Computation, *International Journal of Heat and Mass Transf*, *81* (2015), Feb., pp. 63-74
[15] Hunter, B., Guo, Z., Applicability of Phase-Function Normalization Techniques for Radiation Transfer Computation, *Numererical Heat Transfer (Part B)*, *67* (2015), 1, pp. 1-24
[16] Ren, Y. T., *et al*., Estimation of Radiative Parameters in Participating Media Using Shuffled Frog Leaping Algorithm, *Thermal Science*, *21* (2017), 6, pp. 2287-2297
[17] Chai, J. C., *et al*., Finite Volume Method for Radiation Heat Transfer, *AIAA J. Thermophys Heat Transfer*, *8* (1994), 3, pp. 419-425
[18] Raithby, G. D., Chui, E. H., A Finite-Volume Method for Predicting Radiant Heat Transfer in Enclosures with Participating Media, *ASME Journal of Heat Transfer*, *112* (1990), 2, pp. 415-423
[19] Chai, J. C., *et al*., Finite-Volume Method for Radiation Heat Transfer, *Journal of Thermophysics and Heat Transfer*, *8* (2000), 3, pp. 419-425
[20] Chai, J. C., *et al.*, Treatment of Irregular Geometries Using a Cartesian-co-Ordinates-Based Discrete-Ordinates-Method, *Radiation Heat Transfer Theory and Application HTD*, *244* (1993), pp. 49-54
[21] Coelho, P. J., Bounded Skew High-Order Resolution Schemes for the Discreteordinates Method, *Journal of Computational Physics*, *175* (2002), 2, pp. 412-437
[22] Guedri, K., *et al*., Application of High-Resolution NVD Differencing Schemes to the FT*n* Finite Volume Method for Radiative Heat Transfer, *Heat Transfer-Asian Reserach*, *47* (2018), 2, pp. 366-388

[23] Guedri, K., Al-Ghamdi, A. S., Radiative Heat Transfer in Complex Enclosures Using NVD Differencing Schemes of the FT*n* Finite Volume Method, *Heat Transfer Research*, *48* (2017), 15, pp. 1379-1398
[24] Guedri, K., *et al*., Numerical Study of Radiative Heat Transfer Effects on a Complex Configuration of Rack Storage Fire, *Energy*, *36* (2011), 5, pp. 2984-2996
[25] Coelho, P. J., Aelenei, D., Application of High-Order Spatial Resolution Schemes to the Hybrid Finite Volume/Finite Element Method for Radiative Transfer in Participating Media, *International Journal of Numererical Methods Heat and Fluid-Flow*, *18* (2008), 2, pp. 173-184
[26] Ren, Y. T., *et al*., Estimation of Radiative Parameters in Participating Media Using the Shuffled Frog Leaping Algorithm, *Thermal Science*, *21* (2017), 6A, pp. 2287-2297
[27] Byun, D., *et al*., Radiative Heat Transfer in Discretely Heated Irregular Geometry with an Absorbing, Emitting, and Anisotropically Scattering Medium Using Combined Monte-Carlo and Finite Volume Method, *International Journal of Heat and Mass Transfer*, *47* (2004), 19-20, pp. 4195-4203
[28] Chai, J. C., Moder, J. P., Radiation Heat Transfer Calculation Using an Angular-Multiblock Procedure, *Numererical Heat Transfer (Part B)*, *38* (2000), 1, pp. 1-13
[29] Kim, S. H., Huh, K.Y., A New Angular Discretization Scheme of the Finite Volume Method for 3-D Radiative Heat Transfer in Absorbing, Emitting and Anisotropically Scattering Media, *International Journal of Heat and Mass Transfer*, *43* (2000), 7, pp. 1233-1242
[30] Guedri, K., *et al*., Evaluation of the FT*n* Finite Volume Method for Transient Radiative Transfer in Anisotropically Scattering Medium, *Numer. Heat Transfer (Part B)*, *68* (2015), 10, pp. 1137-1154
[31] Padhi, B. N., Thermal Modelling of Short Pulse Collimated Radiation in a Participating Medium, Ph. D thesis, The National Institute of Technology, Odisha, India, 2012
[32] Bhowmik, A., *et al*., Analysis of Radiative Signals from Normal and Malignant Human Skins Subjected to a Short-Pulse Laser, *Inter. J. Heat Mass Transfer*, *68* (2014), Jan., pp. 278-294
[33] Modest, M. F., *Radiative Heat Transfer*, 2nd ed., Academic Press, New York, USA, 2003
[34] Guo, Z., Kumar, S., Equivalent Isotropic Scattering Formulation for Transient Short-Pulse Radiative Transfer in Anisotropic Scattering Planar Media, *Appied Optics*, *39* (2000), pp. 4411-4417
[35] Guo, Z., Kim, K., Ultrafast-Laser-Radiation Transfer in Heterogeneous Tissues with the Discreteordinates Method, *Applised Optics*, *42* (2003), 16, pp. 2897-2905

Paper submitted: March 2, 2018
Paper revised: April 17, 2018
Paper accepted: June 5, 2018